

# Vectorized Parallel in Time methods for low-order discretizations with application to Porous Media problems

Christian Engwer<sup>\*1</sup>, Alexander Schell<sup>†1</sup>, and Nils-Arne Dreier<sup>‡1,2</sup>

<sup>1</sup>Applied Mathematics: Institute for Analysis and Numerics, University of Münster,  
Einsteinstr. 62, 48149 Münster, Germany

<sup>2</sup>now at Deutsches Klimarechenzentrum, Bundesstraße 45a, 20146 Hamburg, Germany

## Abstract

High order methods have shown great potential to overcome performance issues of simulations of partial differential equations (PDEs) on modern hardware, still many users stick to low-order, matrix-based simulations, in particular in porous media applications. Heterogeneous coefficients and low regularity of the solution are reasons not to employ high order discretizations.

We present a new approach for the simulation of instationary PDEs that allows to partially mitigate the performance problems. By reformulating the original problem we derive a parallel in time integrator that increases the arithmetic intensity and introduces additional structure into the problem. By this it helps accelerate matrix-based simulations on modern hardware architectures.

Based on a system for multiple time steps we will formulate a matrix equation that can be solved using vectorized solvers like Block Krylov methods. The structure of this approach makes it applicable for a wide range of linear and nonlinear problems. In our numerical experiments we present some first results for three different PDEs, a *linear convection-diffusion equation*, a *nonlinear diffusion-reaction equation* and a realistic example based on the *Richards' equation*.

**Keywords:** Parallel in Time, Hardware-Aware Numerics, Vectorization, Nonlinear, Richards' equation, DIRK methods

**MSC Classification:** 86-08, 65J10, 65J15, 65M20, 65Y05, 65Y10, 49M15, 35K61

## 1 Introduction

In the context of porous media problems, simulations are often on a scale that requires significant computation power. Making good use of the available compute power on modern hardware architectures is thus of high importance.

As of today in porous media simulations low-order methods, like finite-volume or first-order mixed-FE methods, are still the dominant approach, e.g. [7, 17, 26, 18, 16], and are usually following the classical way of a nonlinear Newton-type solver with an embedded iterative linear solver, where the latter is most often matrix based. One reason for the matrix based workflow is that it allows focussing on the modelling, while the solver *simply works*. A second reason is the use of strong preconditioners, which often require a matrix to set up, e.g. ILU or AMG preconditioners.

As a consequence these methods are memory bandwidth limited and show a low arithmetic intensity (AI), i.e. the ratio between floating point operations per transferred byte. This reduces their efficiency on modern hardware significantly.

The aim of this work is to offer a relatively lightweight approach to reformulate the existing methods in a way that improves hardware efficiency without modifying the spatial discretization. The central idea is to modify the time-integration method.

---

\*christian.engwer@uni-muenster.de

†Corresponding author: alexander.schell@uni-muenster.de

‡dreier@dkrz.de

**Efficiency challenges** Regarding efficient computations on modern hardware one thus faces two major problems. As the memory bandwidth is growing slower than the FLOP rate, low-order methods can not fully benefit from the hardware evolution. The second problem is an increasing concurrency. While many codes support the parallel simulation using multiple threads or processes, the data level parallelism, offered by SIMD (Single Instruction Multiple Data) and wide-SIMD units, requires sufficient structure in the numerical method. In the end, these problems hold true to CPUs just as well as GPUs.

The main computational costs are in the linear solver, which is usually bandwidth limited, due to the inherently low arithmetic intensity of the sparse matrix-vector product (`spMV`). For a double precision calculation two FLOP (one multiply and one add) are performed for two transferred `double` values (one matrix entry, one vector entry); the result entry is written multiple time, so we might neglect it here. All in all we obtain  $\text{AI}(\text{spMV}) = \frac{1}{8}$ , which means that the actual compute power is not used at all and on many modern computers we obtain only fraction of the peak-performance. The advertised peak performance of an *Intel Xeon Gold 6148 @ 2.40 GHz* is 1024 GFlop/s<sup>1</sup>. Since it has 20 cores, the peak performance of a single core is 51.2 GFlop/s. Without AVX512 and FMA this reduces to 3.2 GFlop/s. Therefore, classical non-parallel code is bound by 3.2 GFlop/s and you loose > 99% of performance.

**Increasing the Arithmetic Intensity** Not modifying the spatial discretization, two approaches to increase the Arithmetic Intensity are possible.

One way to partially mitigate this problem is to use mixed-precision calculations, e.g. by applying the preconditioner in single precision and only calculate the residual in double precision. By this one is able to reduce the transfer costs, but still this increases AI, and by this the actual performance, by less than a factor 2. At the same time one has to be very careful to ensure that the reduced precision does neither impede the overall convergence and does not introduce stability issues. For an overview of mixed-precision methods and their analysis we refer to the review article by [13]. In [11] it is discussed how to apply mixed-precision algorithms to Runge-Kutta schemes.

An alternative approach is possible whenever a set of different linear systems with the same left-hand-side operator, but different right-hand-sides, needs to be solved. Examples are certain multi-scale methods, like MsFEM [15] and LOD [9], certain inverse problems [21, 27] or the randomized construction of low-rank approximations [22]. Such a system can be reformulated to solve a single matrix equation instead of many linear systems with different right-hand-sides. The arising system takes the form

$$AX = B, \tag{1}$$

where  $A \in \mathbb{R}^{N \times N}$  and  $X, B \in \mathbb{R}^{N \times k}$  for some  $k \in \mathbb{N}$ , and can be solved using Block Krylov methods, which were first presented by [23]. They show better convergence behaviour, due to information exchange between the columns. Recently Block Krylov methods got rediscovered to mitigate the communication overhead on high performance systems [12]. Their important feature is that they increase the arithmetic intensity and directly expose a vectorized structure [8, 3, 20]. This is what the approach in this paper builds upon.

**Main Contribution and Structure of the paper** The main contribution of this paper is to provide a new framework for the implicit solvers for instationary PDEs of the form

$$\begin{aligned} My(t) + Ky(t) &= b(t) \quad \text{for } t > 0, \\ y(0) &= y_0, \end{aligned} \tag{2}$$

where  $K \in \mathbb{R}^{N \times N}$  is the stiffness matrix,  $b(t) \in \mathbb{R}^N$  a right-hand-side vector and mass matrix  $M \in \mathbb{R}^{N \times N}$ . In particular, such systems occur at the discretization of parabolic PDEs using the method of lines.

The new approach picks up ideas from parallel in time methods (PinT). We transform the original problem into a space-time problem, considering multiple time steps at once. A similar approach was already presented by [6]. In contrast to the traditional PinT paradigm we do not consider large time slaps and aim for a global parallelization over the time steps, but instead parallelize over consecutive time steps or Runge-Kutta stages to increase the node-level performance and employ vectorization. Vectorization is omnipresent on modern architectures via SIMD and wide-SIMD units, e.g. AVX and AVX-512 on x64 CPUs. To fully employ SIMD Units, additional structure is needed. We present a *matrix splitting*

---

<sup>1</sup>APP Metrics for Intel® Microprocessors - Intel® Xeon® Processor

*approach* to achieve this structure and formulate a matrix equation for solving the consecutive time steps. This matrix equation can then be solved by a vectorized Block Krylov method [8].

The method is fairly general and is especially well suited for stiffly accurate DIRK methods (*diagonally implicit Runge-Kutta*) methods.

This paper is structured as follows. In Section 2 we deduce the framework in an abstract way. In Section 3 we explain the expected convergence behaviour with a simple performance model. Three numerical examples based on three different PDEs are presented in Section 4. We conclude the work in Section 5 and give a short outlook for further investigations.

## 2 Vectorized time integrators

For the time discretization of problem (2) consider the generic class of  $m$  - stage diagonally implicit Runge-Kutta methods (DIRK methods). These methods can be described by their Butcher tableau of the form

$$\begin{array}{c|cccc} c_1 & a_{1,1} & & & \\ c_2 & a_{2,1} & a_{2,2} & & \\ c_3 & a_{3,1} & a_{3,2} & a_{3,3} & \\ \vdots & \vdots & \vdots & \vdots & \ddots \\ c_m & a_{m,1} & a_{m,2} & a_{m,3} & \dots & a_{m,m} \\ \hline & b_1 & b_2 & b_3 & \dots & b_m \end{array}$$

respectively the matrix  $A \in \mathbb{R}^{m \times m}$  and the vectors  $b, c \in \mathbb{R}^m$ . We focus on *stiffly accurate* methods that is methods satisfying the following property

$$b_i = a_{m,i} \quad \forall i = 1, \dots, m.$$

Let  $y^{(n,k)} \approx y(t^n + c_k \tau)$  be the  $k$ -th stage of the  $n$ -th time step of the method and let  $t^{(n,k)} = t^n + c_k \tau$  denote its corresponding time point. Then a stiffly accurate DIRK method to solve (2) reads as

$$\begin{aligned} y^{(n,1)} &= y^n \\ \frac{1}{\tau} M(y^{(n,k)} - y^n) + \sum_{j=1}^k a_{ij} K y^{(n,j)} &= \sum_{j=1}^k a_{i,j} b(t^{(n,j)}), \quad \forall k = 1, \dots, m \\ y^{n+1} &= y^{(n,m)} \end{aligned} \tag{3}$$

with time step width  $\tau > 0$ .

### 2.1 Matrix equation formulation

To formulate a matrix equation for all stages, one reformulates the system (3) into an all-at-once system, as typically done in *PinT*-methods. Using the Kronecker product  $\otimes$  the system for the  $m$  stages of a stiffly accurate DIRK method can be written as

$$[A_1 \otimes M + A_2 \otimes K] \text{vec}(Y) = [A_2 \otimes \mathbb{I}_N] \text{vec}(B) + \text{vec}(B_0), \tag{4}$$

where  $Y, B \in \mathbb{R}^{N \times m}$  are defined as

$$Y = (y^{(n,1)}, \dots, y^{(n,m)}) \quad \text{and} \quad B = (b^{(n,1)}, \dots, b^{(n,m)})$$

and  $\text{vec}(X) = (X_1^T, \dots, X_s^T)^T \in \mathbb{R}^{(Nm)}$  denotes the stacked column vector of  $X \in \mathbb{R}^{N \times m}$ . The time stepping matrices  $A_1, A_2 \in \mathbb{R}^{m \times m}$  and  $B_0 \in \mathbb{R}^{N \times m}$  depend on the particular DIRK method and are defined via the Butcher tableau

$$A_1 = \frac{1}{\tau} \mathbb{I}_m \quad , \quad A_2 = A \quad \text{and} \quad B_0 = \frac{1}{\tau} (M y^n, \dots, M y^n).$$

In the case of an explicit first stage, i.e.  $a_{1,1} = 0$ , it is clear that  $y^{(n,1)} = y^n$  and thus no linear system needs to be solved for this stage. Instead,  $y^{(n,1)}$  can be moved to the right-hand-side directly.

Moreover, this effects the structure of the time stepping matrix  $A_2$  and is well-suited for the *matrix splitting approach* we present later. We illustrate this for general Runge-Kutta schemes. That is for schemes of the form

$$\begin{array}{c|ccc} 0 & 0 & \vdots & \\ \cdots & \cdots & \cdots & \\ c_2 & a_{21} & \vdots & \\ \vdots & \vdots & \vdots & A_{\text{impl}} \\ c_m & a_{m1} & \vdots & \\ \hline & b_1 & b_2 & \cdots & b_m \end{array}$$

with  $A_{\text{impl}} \in \mathbb{R}^{(m-1) \times (m-1)}$ . Based on (3) the system for the stages is given by

$$\begin{aligned} \left[ \frac{1}{\tau} \begin{pmatrix} 1 & 0 & \cdots & 0 \\ 0 & \vdots & \vdots & \vdots \\ \vdots & \vdots & \mathbb{I}_{m-1} & \vdots \\ 0 & \vdots & \vdots & \vdots \end{pmatrix} \otimes M + \begin{pmatrix} 1 & 0 & \cdots & 0 \\ a_{21} & \vdots & \vdots & \vdots \\ \vdots & \vdots & A_{\text{impl}} & \vdots \\ a_{m1} & \vdots & \vdots & \vdots \end{pmatrix} \otimes K \right] \begin{pmatrix} y^{(n,1)} \\ y^{(n,2)} \\ \vdots \\ y^{(n,m)} \end{pmatrix} \\ = \left[ \begin{pmatrix} 1 & 0 & \cdots & 0 \\ a_{21} & \vdots & \vdots & \vdots \\ \vdots & \vdots & A_{\text{impl}} & \vdots \\ a_{m1} & \vdots & \vdots & \vdots \end{pmatrix} \otimes \mathbb{I}_N \right] \begin{pmatrix} b^{(n,1)} \\ b^{(n,2)} \\ \vdots \\ b^{(n,m)} \end{pmatrix} + \frac{1}{\tau} \begin{pmatrix} My^n \\ My^n \\ \vdots \\ My^n \end{pmatrix} \end{aligned}$$

Using the identity  $y^{(n,1)} = y^n$  the corresponding first row can be eliminated and the couplings to  $y^{(n,1)}$  are moved to the right-hand-side. This yields

$$\begin{aligned} \left[ \frac{1}{\tau} \mathbb{I}_{m-1} \otimes M + A_{\text{impl}} \otimes K \right] \begin{pmatrix} y^{(n,2)} \\ \vdots \\ y^{(n,m)} \end{pmatrix} \\ = [A_{\text{impl}} \otimes \mathbb{I}_N] \begin{pmatrix} b^{(n,2)} \\ \vdots \\ b^{(n,m)} \end{pmatrix} + \frac{1}{\tau} \begin{pmatrix} My^n \\ \vdots \\ My^n \end{pmatrix} + \begin{pmatrix} a_{21}(b^n - Ky^n) \\ \vdots \\ a_{m1}(b^n - Ky^n) \end{pmatrix} \end{aligned}$$

above (4) for a DIRK method which is exactly of the form described of one stage less and couplings to the eliminated stage represented by additional contributions in  $B_0$ .

**Example 1.** *Eliminating the first stage of the  $\Theta$ -method this yields its well known form*

$$\left( \frac{1}{\tau} M + \Theta K \right) y^{n+1} = \Theta b^{n+1} + \frac{1}{\tau} My^n + (1 - \Theta)(b^n - Ky^n),$$

which will be used in the later numerical experiments in Section 4.

These concepts can easily be extended such that not only  $m$  stages of a single time step are considered, but also  $s$  consecutive time steps, each consisting of  $m$  stages. This is directly achieved by extending the matrices  $A_1, A_2$  to block matrices in  $\mathbb{R}^{(s \cdot m) \times (s \cdot m)}$  and  $B_0$  to  $\mathbb{R}^{N \times (s \cdot m)}$ , leading to the following matrices

$$\begin{aligned} A_1 &= \frac{1}{\tau} \begin{pmatrix} \mathbb{I}_m & & \\ & \ddots & \\ & & \mathbb{I}_m \end{pmatrix}, \quad A_2 = \begin{pmatrix} A & & \\ & \ddots & \\ & & A \end{pmatrix} \quad \text{and} \\ B_0 &= \frac{1}{\tau} \left( \underbrace{My^n, \dots, My^n}_m, \dots, \underbrace{My^{n+s-1}, \dots, My^{n+s-1}}_m \right), \end{aligned}$$

with potentially additional terms in  $B_0$  if an explicit stage was eliminated before. Note that the  $y^{n+i}, i = 1, \dots, s-1$  are in general unknown, but for the stiffly accurate methods it holds that

$$y^{n+i} = y^{(n+i-1, m)}, \quad i = 1, \dots, s-1$$

and hence the corresponding dependencies are already included in the left-hand-side operator. The matrices therefore will look as follows

$$A_1 = \left( \begin{array}{c|ccc} \mathbb{I}_m & & & \\ \hline & -1 & & \\ & \vdots & \mathbb{I}_m & \\ & -1 & & \\ \hline & & & -1 \\ & & & \vdots \\ & & & -1 \end{array} \right), \quad (5)$$

$$A_2 = \left( \begin{array}{c|ccc} A & & & \\ \hline & A & & \\ & & & \ddots \end{array} \right) \quad \text{and} \quad B_0 = \frac{1}{\tau} \left( \underbrace{My^n, \dots, My^n}_m, 0, \dots \right).$$

If an explicit stage was eliminated,  $A_2$  will as well carry the additional entries  $a_{2,1}, \dots, a_{m,1}$  in the same positions as the  $-1$  entries in  $A_1$  and  $B_0$  will also contain the additional terms in the first  $m$  columns. In Example 2 we show how these matrices  $A_1, A_2$  and  $B_0$  will look like for the  $\Theta$ -method.

From now on, for simplicity we assume that only a single time step consisting of  $m$  stages is considered, but all concepts can be canonically extended to the more complex case of multiple time steps. Later, the main ideas are shown by the use of some examples.

**Example 2.** (*Time stepping matrices for  $\Theta$ -method*) Considering  $s$  consecutive time steps of the  $\Theta$ -method after eliminating the explicit stage the time stepping matrices  $A_1, A_2 \in \mathbb{R}^{s \times s}$  and the right-hand-side  $B_0 \in \mathbb{R}^{N \times s}$  are given by

$$A_1 = \frac{1}{\tau} \begin{pmatrix} 1 & & & & \\ -1 & 1 & & & \\ & & \ddots & \ddots & \\ & & & -1 & 1 \end{pmatrix}, \quad A_2 = \begin{pmatrix} \Theta & & & & \\ 1 - \Theta & \Theta & & & \\ & & \ddots & \ddots & \\ & & & 1 - \Theta & \Theta \end{pmatrix},$$

$$B_0 = \left( \frac{1}{\tau} My^n - (1 - \Theta)(Ky^n - b^n), \quad 0, \quad \dots, \quad 0 \right).$$

To apply vectorized Block Krylov methods to the resulting system it must be ensured that (4) can be transformed into a matrix equation. Therefore, for matrices  $A \in \mathbb{R}^{N \times N}$  and  $X, B \in \mathbb{R}^{N \times m}$ , recall the general identity

$$\begin{pmatrix} A & & \\ & \ddots & \\ & & A \end{pmatrix} \begin{pmatrix} X_1^T \\ \vdots \\ X_m^T \end{pmatrix} = \begin{pmatrix} B_1^T \\ \vdots \\ B_m^T \end{pmatrix}$$

$$\Leftrightarrow (\mathbb{I}_m \otimes A) \text{vec}(X) = \text{vec}(B)$$

$$\Leftrightarrow AX = B.$$

Thus, instead of solving multiple linear system with the same matrix  $A$  we can solve a matrix equation of the form (1). To obtain the desired structure for the left-hand-side operator we propose a *matrix splitting approach* that allows us to decouple the stages in the operator, moving any off-diagonal entry to the right-hand-side. Split the matrices  $A_1$  and  $A_2$  into their diagonal and off-diagonal parts

$$A_1 = \frac{1}{\tau} \mathbb{I}_m + (A_1 - \frac{1}{\tau} \mathbb{I}_m) \quad \text{and} \quad A_2 = \beta \mathbb{I}_m + (A_2 - \beta \mathbb{I}_m), \quad (6)$$

with  $\beta = A_{2(0,0)}$  the entry in the top left corner of the matrix and move all off-diagonal parts to the

right-hand-side of the equation. Equation (4) then can be written as

$$\begin{aligned} & \left[ \frac{1}{\tau} \mathbb{I}_m \otimes M + \beta \mathbb{I}_m \otimes K \right] \text{vec}(Y) \\ & = - \left[ (A_1 - \frac{1}{\tau} \mathbb{I}_m) \otimes M + (A_2 - \beta \mathbb{I}_m) \otimes K \right] \text{vec}(Y) + [A_2 \otimes \mathbb{I}_N] \text{vec}(B) + \text{vec}(B_0), \end{aligned}$$

which has an equivalent matrix equation formulation

$$\left( \frac{1}{\tau} M + \beta K \right) Y = -MY(A_1 - \frac{1}{\tau} \mathbb{I}_m)^T - KY(A_2 - \beta \mathbb{I}_m)^T + BA_2^T + B_0.$$

Due to the splitting, the derived matrix equation has a right-hand-side depending on the solution  $Y$ . Therefore, it cannot be solved directly with a vectorized Block Krylov solver but has to be solved iteratively, e.g. using a fix-point iteration. During this iteration the actual matrix equation then can be solved using a vectorized solver

$$\left( \frac{1}{\tau} M + \beta K \right) Y^j = -MY^{j-1}(A_1 - \frac{1}{\tau} \mathbb{I}_m)^T - KY^{j-1}(A_2 - \beta \mathbb{I}_m)^T + BA_2^T + B_0 \quad (7)$$

**Remark 1.** Let the mass matrix  $M$  be a scaled identity and the left-hand-side operator take the form

$$D \otimes M + \beta \mathbb{I}_m \otimes K,$$

with  $D \in \mathbb{R}^{m \times m}$  a diagonal matrix. In that case one can apply vectorized Block Krylov methods, even though the problem is not in the form of a matrix equation. The reason is that the Block Krylov space of  $(D \otimes M + \beta \mathbb{I}_m \otimes K)$  is the same as that of  $(D_{00}M + \beta K)$ .

**Remark 2.** If one considers the matrix splitting (6) e.g. for the time stepping matrices of the  $\Theta$ -method from Example 2, one realizes that eliminating the explicit stage leads to a smaller splitting error since all zero diagonal entries were removed.

## 2.2 Extension to the nonlinear case

For nonlinear problems, the stiffness matrix has to be replaced by a nonlinear operator  $\mathcal{K}$ . The nonlinear version of the semi-discretized system (2) then reads

$$M\dot{y}(t) + \mathcal{K}(y(t)) = b(t).$$

After linearizing  $\mathcal{K}$  at  $y(t)$  this corresponds to solve

$$M\dot{y}(t) + K[y(t)]y(t) = b(t),$$

with stiffness matrix  $K[y(t)] \in \mathbb{R}^{N \times N}$  or equivalently with  $f(t, y(t)) := K[y(t)]y(t) - b(t)$

$$M\dot{y}(t) + f(t, y(t)) = 0.$$

Thus, the stiffness matrix will differ between the time steps since different linearization points are used. To formulate the matrix equation in this case we introduce another splitting, which ensures that the left-hand-side operator is the same for all time steps. Similar to [6] we use an approximate  $\tilde{K}$  for every time steps. Whilst they propose to define  $\tilde{K}$  as the average over all stiffness matrices, we will use the stiffness matrix of the first time step. In the same fashion as before one can formulate a system for the  $m$  parallel stages of a stiffly accurate DIRK method using the Kronecker product

$$[A_1 \otimes M + (A_2 \otimes \mathbb{I}_N)K] \text{vec}(Y) = [A_2 \otimes \mathbb{I}_N] \text{vec}(B) + \text{vec}(B_0), \quad (8)$$

with  $K$  defined as

$$K := \begin{pmatrix} K[y^{(n,1)}] & & \\ & \ddots & \\ & & K[y^{(n,m)}] \end{pmatrix} := \begin{pmatrix} K^{(n,1)} & & \\ & \ddots & \\ & & K^{(n,m)} \end{pmatrix}.$$

Since equation (8) needs to be transformed into a matrix equation as done in the linear case, as before a splitting has to be applied. Additionally, one needs to ensure that the same stiffness matrix, i.e. the

same linearization is used for every stage. Therefore, similar to [6] we use an approximate  $\tilde{K}$  for all stages. While they suggest constructing  $\tilde{K}$  by averaging, we propose to use the Jacobian of the first stage, similar to the reuse of the Jacobian in simplified Newton methods. For each stage or time step we split the individual Jacobian matrices  $K^{(n,i)}$  as follows

$$K^{(n,i)} = K^{(n,1)} + \tilde{K}^{(n,i)}.$$

With the abbreviated notation  $\tilde{K} := \begin{pmatrix} \tilde{K}^{(n,1)} & & \\ & \ddots & \\ & & \tilde{K}^{(n,m)} \end{pmatrix}$  one gets the following identity  $K = (\mathbb{I}_m \otimes K^{(n,1)}) + \tilde{K}$ , which allows for a split reformulation of system (8) as follows

$$\begin{aligned} \left[ A_1 \otimes M + \underbrace{(A_2 \otimes \mathbb{I}_N)(\mathbb{I}_m \otimes K^{(n,1)})}_{=(A_2 \otimes K^{(n,1)})} \right] \text{vec}(Y) = & - \left[ (A_2 \otimes \mathbb{I}_N) \tilde{K} \right] \text{vec}(Y) \\ & + \left[ A_2 \otimes \mathbb{I}_N \right] \text{vec}(B) + \text{vec}(B_0). \end{aligned} \quad (9)$$

Up to the additional correction term of the Jacobian on the right-hand-side, this is the same formulation as in the linear case (4). Hence, from now on one can apply the same splitting as done in the linear case to obtain the matrix equation formulation

$$\begin{aligned} \left( \frac{1}{\tau} M + \beta K^{(n,1)} \right) Y = & - \left( \tilde{K}^{(n,1)} y^{(n,1)}, \dots, \tilde{K}^{(n,m)} y^{(n,m)} \right) A_2^T \\ & - MY(A_1 - \frac{1}{\tau} \mathbb{I}_m)^T \\ & - K^{(n,1)} Y(A_2 - \beta \mathbb{I}_m)^T + BA_2^T + B_0. \end{aligned} \quad (10)$$

As in the linear case, equation (10) has a solution dependent right-hand-side and thus needs to be solved iteratively, but instead of solving the matrix equation exactly, we will fuse the fix-point iteration with the outer Newton update. We use one iteration of the fix-point problem as the search direction in the outer Newton solver. Due to the mostly explicit structure of the DIRK methods, i.e. stages only couple with previous stages, there is no splitting needed for the left-hand-side operator of the first stage when choosing the Jacobian of the first stage as the approximate Jacobian for all stages. Thus, it is to be expected that the first stage converges fastest, and we employ a so-called *pipelining strategy*, shifting to the next stage, whenever the first stage has converged. As a consequence, after shifting, the first row in system (8) will then correspond to the next stage and will not necessarily belong to the first stage of a time step. Hence, the matrices  $A_1, A_2, B$  and  $B_0$  actually depend on the stage considered for the top row. We indicate this by an additional index  $A_1^{(n,k)}, A_2^{(n,k)}, B^{(n,k)}$  and  $B_0^{(n,k)}$ . To simplify the consecutive numeration of the stages in that case define the index mapping

$$\begin{aligned} \iota : \mathbb{N} \times \mathbb{N} & \rightarrow \mathbb{N} \times \{1, \dots, m\} \\ (n, k) & \mapsto \left( n + \left\lfloor \frac{k-1}{m} \right\rfloor, k \bmod m \right) \end{aligned}$$

Using this mapping denote the  $m$  successive stages starting from  $y^{(n,k)}$  by  $y^{(n,k)}, \dots, y^{(n,k+m-1)}$ . Especially, this means that some considered stages belong to different time steps, hence we are in a similar situation as described in (5). Given the stages  $y^{(n,1)}, \dots, y^{(n,k-1)}$  the matrix equation (10) for  $Y^{(n,k)} = (y^{(n,k)}, \dots, y^{(n,k+m-1)})$  formulates as

$$\begin{aligned} \left( \frac{1}{\tau} M + \beta^{(n,k)} K^{\iota(n,k)} \right) Y^{(n,k)} & \\ = & - \left( \tilde{K}^{\iota(n,k)} y^{\iota(n,k)}, \dots, \tilde{K}^{\iota(n,k+m-1)} y^{\iota(n,k+m-1)} \right) A_2^{(n,k)T} \\ & - MY^{(n,k)} (A_1^{(n,k)} - \frac{1}{\tau} \mathbb{I}_m)^T - K^{\iota(n,k)} Y^{(n,k)} (A_2^{(n,k)} - \beta^{(n,k)} \mathbb{I}_m)^T \\ & + B^{(n,k)} A_2^{(n,k)T} + B_0^{(n,k)}, \end{aligned} \quad (11)$$

where  $A_1^{(n,k)}$  and  $A_2^{(n,k)} \in \mathbb{R}^{m \times m}$  the  $m \times m$  submatrices from (5) starting at the index  $(k, k)$ . The  $i$ -th column of the right-hand-side  $B_0^{(n,k)}$  is given by

$$B_{0_i}^{(n,k)} = \begin{cases} \sum_{j=1}^{k-1} a_{i,j} f(t^n + \tau c_j, y^{(n,j)}) + \frac{1}{\tau} M y^n & \text{if } i+k \leq m+1 \\ 0 & \text{else.} \end{cases}$$

Taking a closer look at the matrix equation (11), one observes that the residual of this equation is given by

$$\mathcal{R}(Y^{(n,k)}) := MY^{(n,k)}A_1^{(n,k)T} - \mathcal{F}(t1^T + \tau c, Y^{(n,k)})A_2^{(n,k)T} - B_0^{(n,k)},$$

where  $\mathcal{F} : \mathbb{R}^m \times \mathbb{R}^{N \times m} \rightarrow \mathbb{R}^{N \times m}$  is the vectorization of  $f(t, y(t)) := K[y(t)]y(t) - b(t)$  from (2), given by

$$\mathcal{F}(T, Y) = (f(T_1, Y_1), \dots, f(T_m, Y_m)) \in \mathbb{R}^{N \times m}.$$

The pseudocode is presented in Algorithm 1 and is described in the following. The algorithm starts by initializing  $Y^{(0,0)}$ . An outer loop loops over all time steps and an inner loop loops over all stages, i.e. handles the pipelining and shifts the stages to the left using the function `shift` in line 4.

$$\text{shift}((Y_1, \dots, Y_{s-1}, Y_s)) = (Y_2, \dots, Y_s, Y_s)$$

Next, the Newton iteration is started, where the residual and the Jacobian are computed as above and finally in line 12 the system is solved using a vectorized solver.

---

**Algorithm 1** Block Krylov Time Stepping with Pipelining

---

```

1:  $Y^{(0,0)} = (y_0, \dots, y_0)$ 
2: for time steps  $n = 0, \dots, \mathbf{do}$ 
3:   for stages  $k = 1, \dots, m$  do
4:      $Y^{(n,k),0} = \text{shift}(Y^{(n,k-1)})$ 
5:     for  $i = 0, \dots$  do
6:        $R \leftarrow \mathcal{R}(Y^{(n,k),i})$ 
7:       if  $\|R_0\| < \varepsilon$  then
8:          $Y^{(n,k)} = Y^{(n,k),i}$ 
9:         break
10:      end if
11:       $J \leftarrow \left( \frac{1}{\tau}M + \alpha_{k,k}Df(t^n + \tau c_k, Y_0^{(n,k),i}) \right)$ 
12:      solve  $JV = R$ 
13:       $Y^{(n,k),i+1} = Y^{(n,k),i} - V$ 
14:    end for
15:  end for
16: end for
```

---

**Remark 3** (Fully-implicit Runge-Kutta methods). *All reformulations shown above that lead to the matrix equation can also be done for fully-implicit Runge-Kutta schemes. The main difference is that for those methods there will be a splitting error in the first stage, hence one cannot guarantee the first stage to converge the fastest which contradicts the assumptions made for the pipelining. In that case one should use an average Jacobian as proposed by [6].*

**Remark 4** (Additional Nonlinearity). *In the case that the underlying problem has an additional non-linearity in the time derivative, which is the case e.g. for Richards' equation (see Section 4), not only the stiffness matrix but also the mass matrix will be time dependent. As a consequence it is necessary to apply the same splitting concepts also to the mass matrix, resulting in an additional splitting error coming from the inexact linearization.*

**Remark 5** (Linearization). *In some cases it might be useful to use a different linearization than the classical Newton method for the spatial part (or the temporal part).*

### 3 Performance analysis

A widely used tool to study the performance of an algorithm is the *arithmetic intensity* (AI), which measures the ratio of computational operations to memory traffic and is defined as the number of *floating-point operations* (FLOPs) per data transferred between memory and processor (measured in *bytes*). A main goal of our approach is to make use of vectorized Krylov solvers to increase the performance by

increasing the arithmetic intensity. In this section we present a short performance analysis for a vectorized Block Krylov method solving

$$AX = B, \quad \text{with } B, X \in \mathbb{R}^{N \times k}.$$

A main ingredient of an iteration of such a method is the BOP kernel, i.e. applying the operator on a block vector

$$Y \leftarrow AX.$$

Compared to the standard sparse matrix-vector product ( $\text{AI}(\text{spMV}) = \frac{1}{8}$ ) this has an increased arithmetic intensity since the matrix only has to be loaded once if we make use of SIMD.

Consider a block-vector  $X \in \mathbb{R}^{N \times k}$  with  $k$  columns. For a double precision calculation two  $2 \cdot k$  FLOP (one multiply and one add for each column) are performed for  $k + 1$  transferred DOUBLE values (one matrix entry and  $k$  block-vector entries). As before, neglect the result entry here. Thus, we obtain an arithmetic intensity of the sparse BOP kernel  $\text{AI}(\text{spBOP}) = \frac{k}{4(k+1)}$ . Figure 1 shows the arithmetic intensity of the sparse BOP kernel for different values of  $k$ . One sees that for  $k = 16$  the arithmetic intensity increased by a factor of about 1.8.

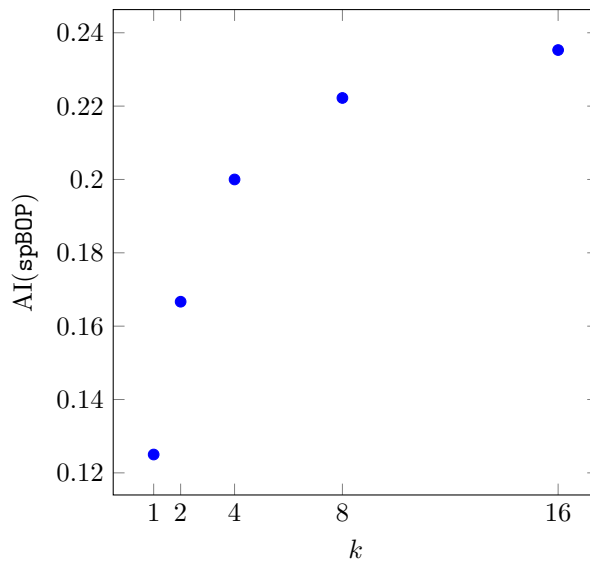


Figure 1: Arithmetic intensity of the sparse BOP kernel for different block sizes.

To analyze the performance of the BOP we consider a simplified variant of the ECM model presented by [14] like in [8], where they assume that the runtime of a kernel is bounded by three factors:

- $T_{\text{comp}} = \frac{\omega}{\text{peakflops}}$ : The time the processor needs to perform the necessary number of floating point operations, with  $\omega$  denoting the number of floating point operations of the kernel.
- $T_{\text{mem}} = \frac{\beta}{\text{memory bandwidth}}$ : The time to transfer the data from the main memory to the L1-cache, with the amount of data that needs to be transferred in the kernel denoted by  $\beta$ .
- $T_{\text{reg}} = \frac{\tau}{\text{register bandwidth}}$ : The time to transfer data between L1-cache and registers. Here  $\tau$  is the amount of data that needs to be transferred in the kernel.

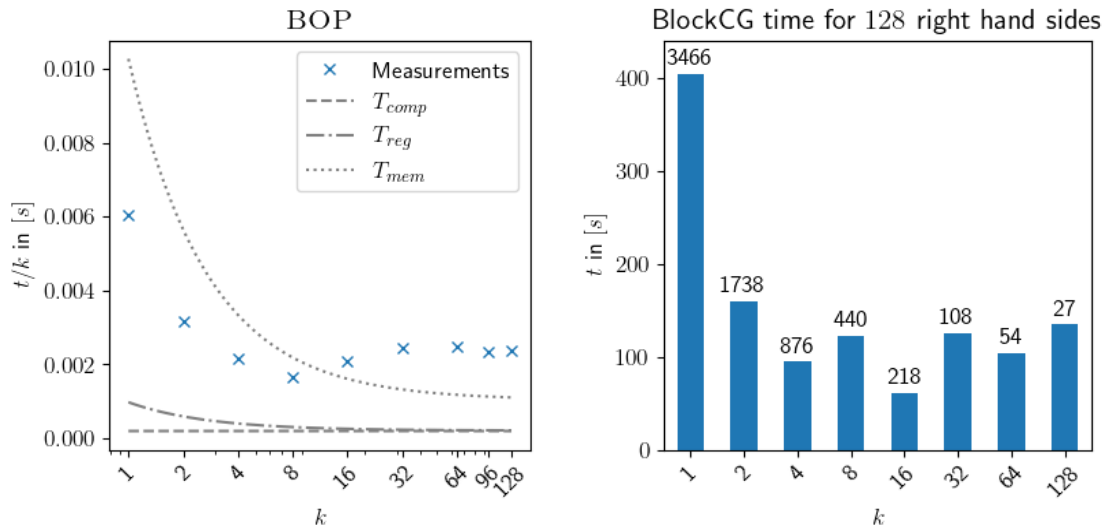
The effective execution time is then given by

$$T = \max(T_{\text{comp}}, T_{\text{mem}}, T_{\text{reg}})$$

We denote by  $\omega$  the number of floating points operations for this kernel, by  $\beta$  the amount of data loaded from main memory and the number of data transfers between registers and L1-cache is given by  $\tau$ . The number of nonzero entries of  $A$  is denoted by  $z$ . In the case of the BOP kernel these characteristics are

given by

$$\begin{aligned}\omega &= 2kz \\ \beta &= 2z + 2kz \\ \tau &= z(2 + 2k)\end{aligned}$$



(a) Measured and expected runtime per right-hand-side of the BOP kernel.

(b) Time needed by the Block-CG to solve for 128 right-hand-sides considering  $k$  right-hand-side in parallel. Numbers on top of the bars denote the number of iterations.

Figure 2: Microbenchmark for the BOP kernel (left) and the Block-CG method (right).

Figure 2a shows the measured runtimes compared to the expected ones. All computations are done on an *Intel Xeon Gold 6148* on a single core. Its theoretical peak performance is 38.4 GFlop/s, the memory bandwidth is 6.39 Gbyte/s and the L1-cache bandwidth is 286.1 Gbyte/s. The microbenchmark for the BOP kernel shows that as expected the runtime per right-hand-side decreases rapidly for small  $k$ . For larger  $k$  the runtime per right-hand-side increases slightly. A reason for this might be that for larger  $k$  one row of a block vector occupies more space in the caches. Thus, fewer rows can be cached resulting in a longer runtime per right-hand-side. Figure 2b further shows the time needed to solve an elliptic PDE for 128 right-hand-sides using a Block-CG Krylov solver with an AMG preconditioner. The exact problem considered is the stiffness matrix of the linearized Richards' equation (see Section 4.3). The required accuracy is a defect reduction of  $10^{-8}$  for all right-hand-sides. One clearly observes a significant reduction in computation time. In this particular case the sweet spot is for  $k = 16$ . Even though fewer iterations are needed when increasing the block size, we do not get faster for  $k$  larger than 16, since each row of a block vector occupies more space in the cache like we observed for the BOP kernel.

**Remark 6** (Nonlinearity). *In addition to discussed benefits in the linear case, we expect a secondary effect in the nonlinear case.*

*Solving (11) with Newton's method, the exact Jacobian is used for the first stage and an approximate Jacobian for any further stages. This means, effectively we perform an exact Newton iteration for the first stage and an inexact Newton iteration for the rest, which introduces a linearization error. Still the inherent splitting error usually dominates the convergence of the outer iteration, i.e. the nonlinear solver. While we don't actually solve the exact nonlinear problem on later stages, still we compute an improved initial guess. This means that after shifting, when a stage become the first one, the initial guess is better than in the sequential case. Often this effect becomes even more prominent for later time steps, resulting in less Newton iterations per stage and an additionally reduced number of linear solver iterations. This can lead to a behaviour where after some initial iterations every stage converges after a single Newton iteration after it has been shifted to the front by the pipelining.*

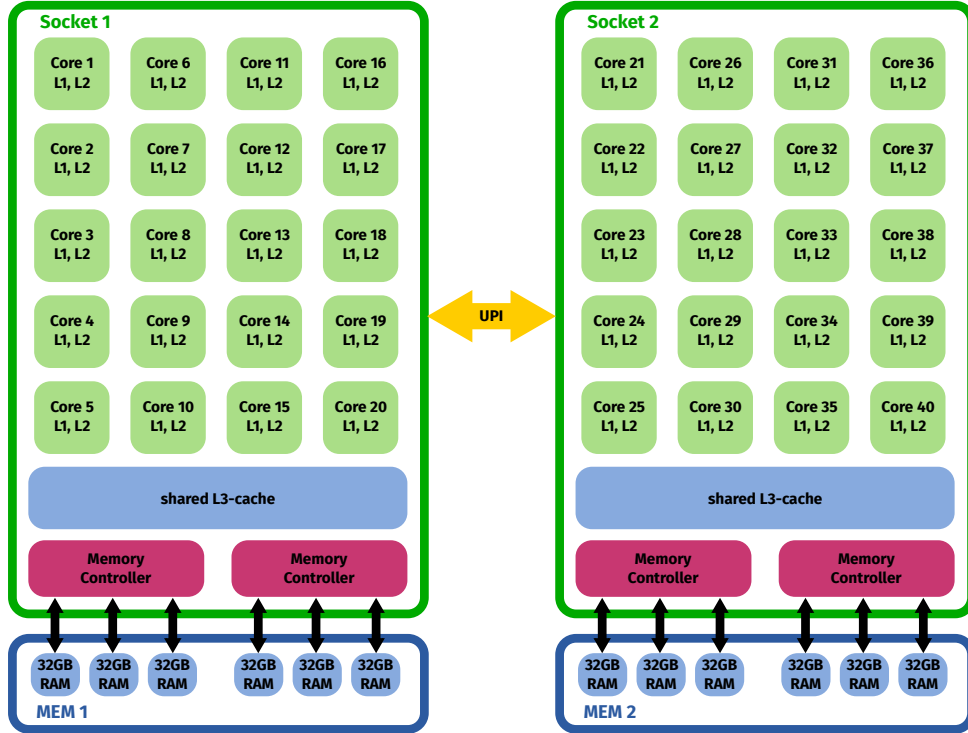


Figure 3: Sketch of the hardware topology of the *Intel(R) Xeon(R) Gold 6148 CPU @ 2.40GHz* used for the numerical experiments. 2 sockets with 20 cores each yields a NUMA layout. Each core has separate L1- and L2-cache, whereas the cores in each socket share one 28 MB L3-cache.

*This clearly depends on the dynamic of the problem we look at. Since we use approximate Jacobians, this behaviour depends on the dynamics of the nonlinear operator  $f$ , i.e. its derivative*

$$\frac{d}{dt}f(t, y(t)).$$

*The more the nonlinear operator changes over time, the worse the approximation error gets we make by choosing the wrong linearization point for the Jacobian.*

## 4 Numerical Experiments

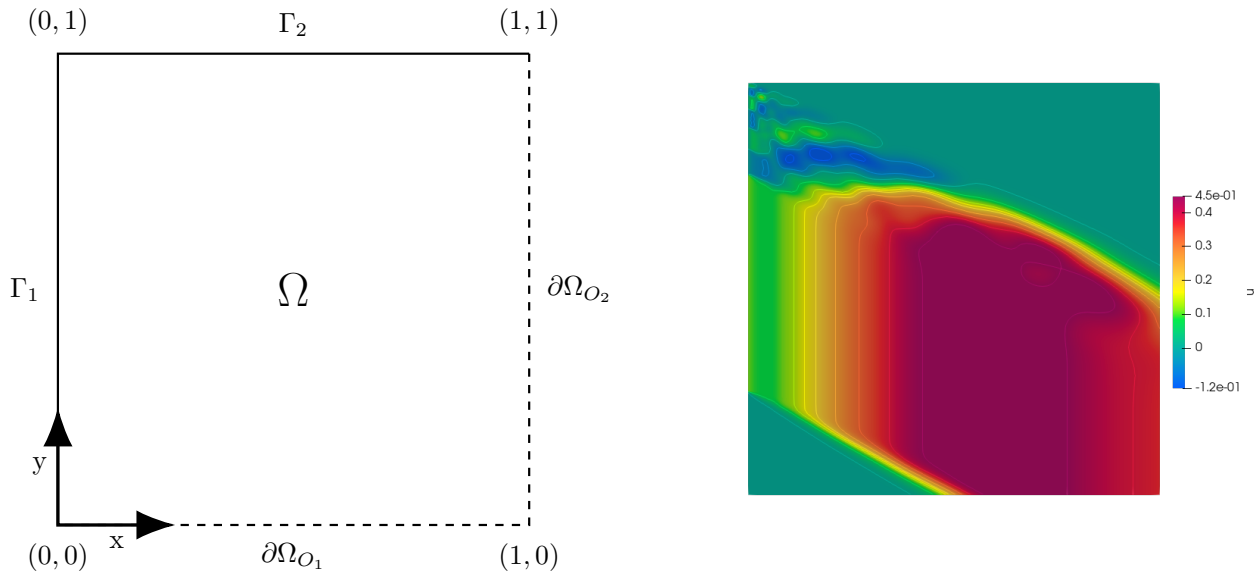
In the numerical experiments we test the method on a series of different problems with growing complexity:

1. Linear Convection-Diffusion
2. Nonlinear Diffusion-Reaction
3. Richards' equation

We implemented a prototype of the pipelining approach presented in section 2 in DUNE [5, 4, 2] where we made use of DUNE's SIMD abstraction to benefit from the SIMD capabilities of the hardware.

All calculations were performed on an *Intel Xeon Gold 6148 CPU @ 2.40GHz* (Intel Skylake) with gcc (11.4.0) and AVX512 support enabled (`-march=skylake-avx512`). The exact hardware topology of the machine is depicted in Figure 3. It consists of two sockets with 20 cores each that have a separate L1- and L2-cache but share the same L3-cache. We ran all of our tests on a single socket, executing 20 identical processes via MPI in order to occupy all cores

```
mpirun -n 20 --bind-to core --map-by core <executable file>
```



(a) Computational domain of the linear convection-diffusion example. Dirichlet boundary is  $\partial\Omega_D = \Gamma_1 \cup \Gamma_2$  and outflow boundary  $\partial\Omega_O = \partial\Omega_{O_1} \cup \partial\Omega_{O_2}$ . (b) Numerical solution for the linear convection-diffusion example at the final time.

Figure 4: Geometry (left) and numerical solution (right) of the linear convection-diffusion example.

This mimics the situation in a productive parallel run, where all cores share a common L3-cache, but compete for the same 6 memory interfaces.

#### 4.1 Linear Convection-Diffusion

The first example considered is a linear convection-diffusion equation

$$\begin{aligned}
 \partial_t u - \nabla \cdot (-A(x)\nabla u + b(x)u) + c(x)u &= 0 && \text{in } \Omega \times (0, T], \\
 u(t, x) &= g(t, x) && \text{on } \partial\Omega_D \times (0, T], \\
 (b(x)u - (A\nabla u)) \cdot n &= 0 && \text{on } \partial\Omega_O \times (0, T], \\
 u(0, x) &= u_0(x) && \text{in } \Omega,
 \end{aligned}$$

where the computational domain is given by  $\Omega = [0, 1]^2$ , the Dirichlet boundary is given by  $\partial\Omega_D = \Gamma_1 \cup \Gamma_2 = \{0\} \times [0, 1] \cup [0, 1] \times \{1\}$  and outflow boundary  $\partial\Omega_O = \partial\Omega \setminus \partial\Omega_D$ . We choose the permeability tensor  $A(x) = 10^{-10} \cdot \mathbb{I}$ , the velocity field  $b(x) = (1, -0.5)^T$  and the reaction term  $c(x) = 1$  to be constant over the whole domain. The Dirichlet boundary condition is given by

$$g(t, x) = \begin{cases} |\sin(2t)|, & \text{if } x \in \{0\} \times \left(\frac{1}{4}, \frac{3}{4} + \frac{1}{4}|\sin(2t)|\right) \\ 0, & \text{else} \end{cases}$$

and the initial distribution is given by  $u_0(x) := g(0, x) = 0$ .

For the spatial discretization we used a cell-centered Finite Volume method (CCFV) on a structured rectangular grid with  $640 \times 640$  elements. The Crank-Nicolson method is used to discretize in time with a time step width of  $\tau = 0.12$ . Simulations were run till the final time  $T = 4.8$ . The solution at the final time generated by our simulations is shown in Figure 4b. If only a single time step is used, the inner and outer tolerances are set to  $1e-8$  which means that every time step converges after a single outer iteration as one would expect. The same could be done when multiple time steps are considered. But in that case we do not expect a huge benefit from our approach since the right-hand-side of the system will be incorrect for all following time steps. Hence, it should be updated frequently. Currently, the only possible way to update the right-hand-side of the system is by adding outer iterations. Therefore, we decided to reduce the inner tolerance  $1e-2$  while the outer tolerance remains untouched. This

means that additional outer iterations are performed for the first time step that allow to update the right-hand-side of the following frequently and result in better preconditioned initial guesses. Another option would be to apply the update of the right-hand-side directly in the inner Krylov-solver, which is part of current research. The matrix equation arising in the outer iteration is solved using a vectorized BLOCK-BICGSTAB implementation from DUNE-ISTL with an AMG preconditioner. Table 1 shows the total number of Newton and Krylov iterations needed and the measured solver times. Figure 5 shows the number of Krylov iterations needed per time depending on the time parallelization.

$s$	Newton It.	Krylov It.	Solver Time	Prec. Setup Time
1	79	713	294.608 [s]	22.429 [s]
2	120	362	161.587 [s]	34.838 [s]
4	81	249	210.039 [s]	24.451 [s]
8	81	246	396.849 [s]	23.716 [s]
16	81	251	692.854 [s]	23.53 [s]

Table 1: Results for the linear problem for  $s$  simultaneously treated time steps of Crank-Nicolson with a total number of 409600 degrees of freedom. All results were computed sequentially on 20 cores on a single socket. Computation times are displayed in seconds.

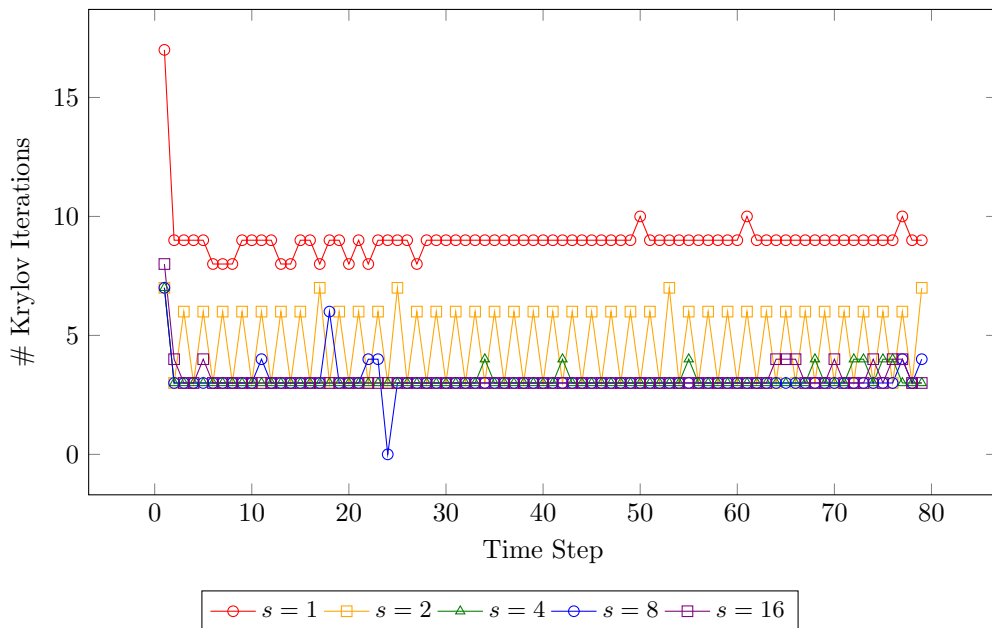


Figure 5: The total amount of inner Krylov iterations needed for each time step when calculating  $s$  consecutive time steps in parallel.

## 4.2 Nonlinear Diffusion-Reaction

The second example is a nonlinear diffusion-reaction equation with Neumann boundary conditions on the unit square  $\Omega = [0, 1]^2$ :

$$\begin{aligned}
 \partial_t u - \nabla \cdot ((1-u)u \nabla u) + \beta(1-u)u &= f && \text{in } \Omega \times (0, T], \\
 \partial_n u(t, x) &= 0 && \text{on } \partial\Omega \times (0, T], \\
 u(0, x) &= u_0(x) && \text{in } \Omega,
 \end{aligned}$$

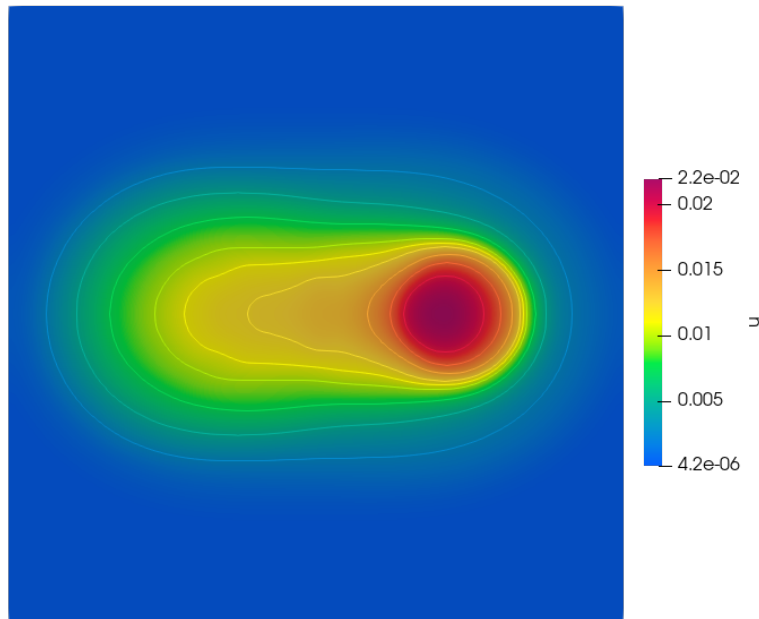


Figure 6: Numerical solution for the nonlinear diffusion-reaction example at the final time.

the initial condition is given by  $u_0(x) = 0.5$ . The parameter  $\beta$  is set to 1 and the source term  $f$  was given by a moving circle

$$f(t, x) = \begin{cases} -0.1, & \text{if } \|x - c\|_2 \leq 0.1 \\ 0, & \text{else,} \end{cases}$$

where the center of the moving circle is given by  $c = (0.5 + 0.25 \cos(6t), 0.5)^T$ . For the spatial discretization we chose  $Q_1$ -Finite Elements on a  $640 \times 640$  rectangular grid. For the temporal discretization Crank-Nicolson with a time step size of  $\tau = 0.12$  is used and the simulation was run till  $T = 9.6$ . The tolerance for the outer iterations was set to  $1e - 8$  and the inner tolerance to  $1e - 5$ . In contrast to the linear case we chose the same inner tolerance for all experiments since due to the nonlinearity we do not need to enforce more outer iterations to update the right-hand-side of the inner system as we did in the linear case. The numerical solution at the final time is shown in Figure 6. Table 2 shows the total number of Newton and Krylov iterations needed for the whole simulation as well as the measured solver times. All linear systems were solved using the BLOCK-CG implementation from DUNE-ISTL with an AMG preconditioner. In Figure 7 both the inner and outer iterations needed for every time step are displayed.

$s$	Newton It.	Krylov It.	Solver Time	Prec. Setup Time
1	278	4,428	1,278.99 [s]	170.13 [s]
2	147	2,354	805.401 [s]	92.485 [s]
4	108	1,717	793.203 [s]	68.554 [s]
8	92	1,479	1,190.36 [s]	59.105 [s]
16	88	1,419	1,914.09 [s]	57.575 [s]

Table 2: Results for the nonlinear diffusion-reaction equation for  $s$  simultaneously treated time steps on a mesh with  $640 \times 640$  elements. All results were computed sequentially on 20 cores on a single socket. Computation times are displayed in seconds.

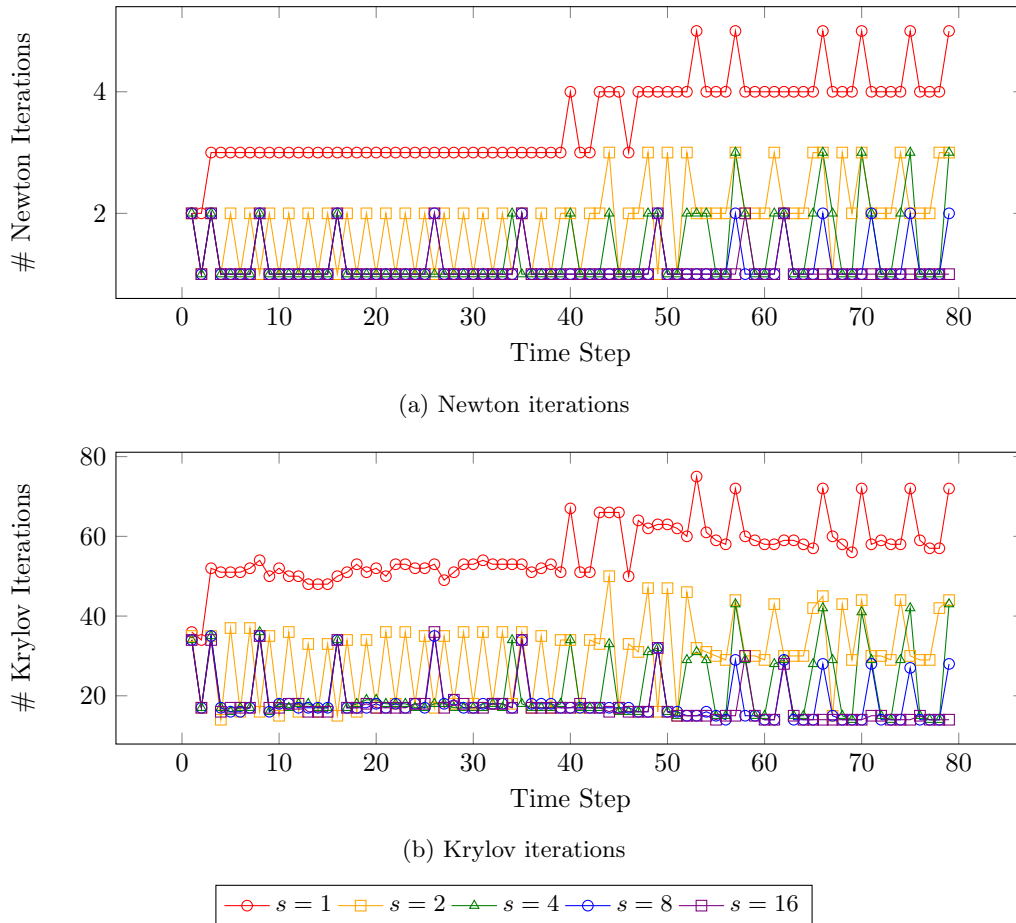


Figure 7: Change of iterations (Nonlinear & Krylov) over the different time steps of the nonlinear diffusion-reaction problem, when considering  $s$  consecutive time steps in parallel.

### 4.3 Richards' equation

The last example is Richards' equation. It models unsaturated flow in soil and reads as

$$\begin{aligned} \partial_t \Theta(\psi) - \nabla \cdot (K(\psi) \nabla(\psi + z)) &= f && \text{in } \Omega \times (0, T], \\ \psi &= g(t, \cdot) && \text{on } \Gamma_D \times (0, T], \\ -K(\psi) (\nabla \psi + e_z) \cdot n &= 0 && \text{on } \Gamma_N \times (0, T] \\ \psi(0, \cdot) &= \psi_0(\cdot) && \text{in } \Omega, \end{aligned}$$

where the primal variable  $\psi$  denotes the pressure head,  $\Theta(\psi)$  the water content,  $K(\psi)$  the conductivity,  $z$  the height against gravitation,  $e_z := \nabla z$  and  $f$  is a source term. The highly nonlinear dependencies between  $K, \Theta$  and  $\psi$  are described based on experimental results, and we use the widely used model of [30]

$$\begin{aligned} \theta(\psi) &= \begin{cases} \theta_R + (\theta_S - \theta_R) \left( \frac{1}{1 + (-\alpha\psi)^n} \right)^{\frac{n-1}{n}} & \text{for } \psi \leq 0 \\ \theta_S & \text{for } \psi > 0 \end{cases} \\ K(\psi) &= K_S \left( \frac{\theta(\psi)}{\theta_S} \right)^{\frac{1}{2}} \left[ 1 - \left( 1 - \left( \frac{\theta(\psi)}{\theta_S} \right)^{\frac{n}{n-1}} \right)^{\frac{n-1}{n}} \right]^2, \end{aligned} \tag{12}$$

where  $\Theta_S$  denotes the water content and  $K_S$  the hydraulic conductivity in the fully saturated medium.  $\Theta_R$  stands for the residual water content and  $\alpha$  and  $n$  are model parameters related to the soil properties. The relationships are shown in Figure 8.

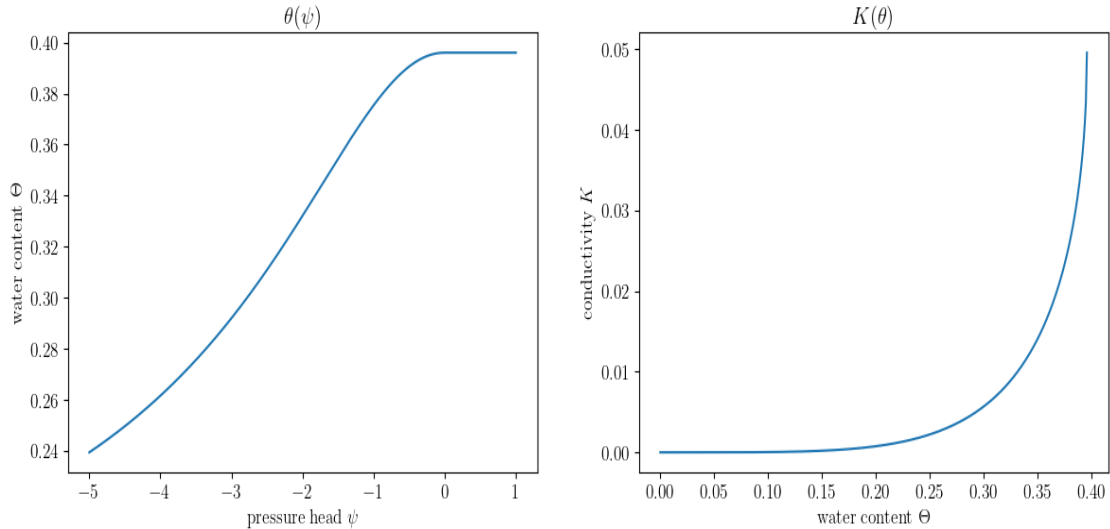
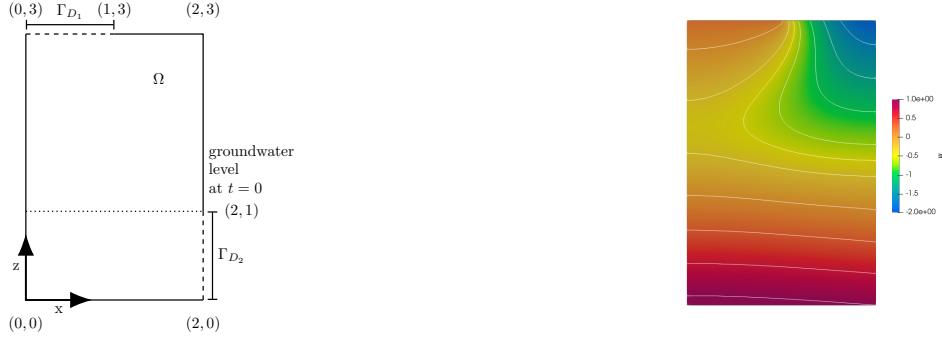


Figure 8: Relationships between  $K, \Theta, \psi$  based on the van Genuchten-Mualem model (12). Soil parameters are taken from Table 3.

In the considered example the Richards' equation will be nonlinear and degenerate elliptic-parabolic. Its solutions typically will have low regularity [1]. The exact setting we use here is a benchmark problem used by e.g. [28, 19] amongst others. It models the recharge of a groundwater reservoir from a drainage trench in two spatial dimensions. The domain  $\Omega \subset \mathbb{R}^2$  represents a vertical cross-section of the subsurface. The groundwater table is fixed by a Dirichlet boundary condition for the pressure height for  $z \in [0, 1]$  on the right-hand-side of  $\Omega$ ,  $\Gamma_{D_2}$ . On the upper boundary of  $\Omega$   $\Gamma_{D_1}$  for  $x \in [0, 1]$  the drainage trench is modelled by a transient Dirichlet condition. On the remaining part of the boundary, no-flow conditions are imposed. The left part of the domain boundary can be interpreted as symmetry axis of the geometry and the lower part of the domain boundary can be seen as transition to an aquitard. The exact geometry is given by



(a) Geometry for the silt loam benchmark problem, from [19]. (b) Numerical solution for the pressure height  $\psi$  after  $4.5h$ .

Figure 9: Geometry (left) and numerical solution at the final time (right) for the benchmark problem of the Richards' equation.

$$\begin{aligned}
\Omega &= (0, 2) \times (0, 3), \\
\Gamma_{D_1} &= \{(x, z) \in \partial\Omega \mid x \in [0, 1] \wedge z = 3\}, \\
\Gamma_{D_2} &= \{(x, z) \in \partial\Omega \mid x = 2 \wedge z \in [0, 1]\}, \\
\Gamma_D &= \Gamma_{D_1} \cup \Gamma_{D_2}, \\
\Gamma_N &= \partial\Omega \setminus \Gamma_D,
\end{aligned}$$

and is illustrated in Figure 9a.

The initial and boundary conditions are given by

$$\begin{aligned}
\psi(t, x, z) &= \begin{cases} -2 + 2.2t/\Delta t_D, & \text{on } \Gamma_{D_1}, t \leq \Delta t_D, \\ 0.2, & \text{on } \Gamma_{D_1}, t > \Delta t_D, \\ 1 - z, & \text{on } \Gamma_{D_2}, \end{cases} \\
-K(\psi(t, x, z))(\nabla\psi(t, x, z) + e_z) \cdot n &= 0 \quad \text{on } \Gamma_N, \\
\psi^0(x, z) &= 1 - z \quad \text{on } \Omega.
\end{aligned}$$

The set of parameters characterizing the soil are taken from [30]. They represent silt loam and are shown in Table 3. For the spatial discretization we choose first order Finite Elements on a mesh with  $400 \times 600$  elements. For the temporal discretization we choose the implicit Euler method. Since Newton's method might fail as shown in [25], we use the *L-Scheme* as the linearization method as done in [19]. The L-Scheme can be interpreted as a quasi-Newton method that uses the monotonicity of  $\Theta$ . It replaces its derivative by a constant  $L$  and was proposed for the Richards' equation by [29, 24, 31]. We use a time step size of  $\tau = \frac{1}{96}$  and perform the simulations until the final time  $T = \frac{3}{16}$ . The parameter for the time evolution of the upper Dirichlet boundary is given by  $\Delta t_D = \frac{1}{16}$ . The L-Scheme parameter  $L$  is chosen to be the Lipschitz constant of  $\Theta$ , that is  $L = 4.501 \cdot 10^{-2}$ . In this example the time unit is 1 day and all spatial dimensions are given in meters. For the stopping criterion of the outer L-Scheme iteration we again refer to [19], where a combination of absolute and relative error is used with absolute and relative tolerances of  $1e - 5$ .

Figure 9b shows the numerical solution at the final time computed with our method and Table 4 shows the total number of L-Scheme iterations and inner Krylov iterations needed together with the total time needed by the linear solver. All arising linear systems were solved using a vectorized BLOCK-CG implementation with an AMG preconditioner. Figure 10 shows the evolution of the L-Scheme iterations and inner Krylov iterations needed for every time step.

Silt loam benchmark problem	
<b>van Genuchten parameters:</b>	
$\Theta_S$	0.396
$\Theta_R$	0.131
$\alpha$	0.423
$n$	2.06
$K_S$	$4.96 \cdot 10^{-2}$

Table 3: Soil parameters for the silt loam benchmark problem [30]

$s$	L-Scheme It.	Krylov It.	Solver Time	Prec. Setup Time
1	139	2,247	367.687 [s]	52.661 [s]
2	75	1,213	195.711 [s]	28.715 [s]
4	49	760	140.13 [s]	17.835 [s]
8	40	550	216.597 [s]	15.416 [s]
16	42	589	316.704 [s]	16.233 [s]

Table 4: Results for the benchmark problem of the Richards' equation for  $s$  simultaneously treated time steps on a mesh with  $400 \times 600$  elements. All results were computed sequentially on 20 cores on a single socket. Computation times are displayed in seconds.

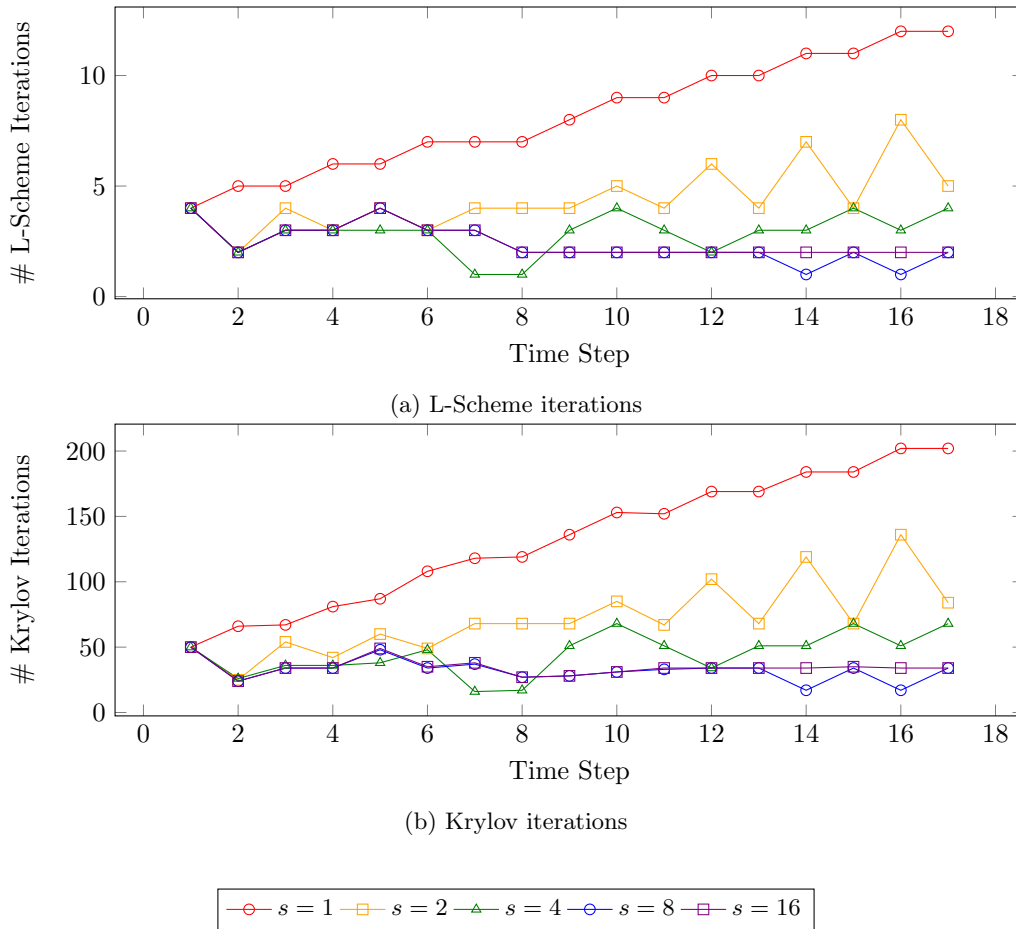


Figure 10: Change of iterations (L-Scheme & Krylov) over the different time steps of the Richards problem, when considering  $s$  consecutive time steps in parallel.

## 4.4 Discussion of the results

The presented numerical experiments show that the total number of linear Krylov iterations and, in the nonlinear case, also the number of Newton iterations has been significantly reduced when computing multiple consecutive time steps in parallel. In the linear case the number of linear iterations was reduced by approximately 50 – 60% (see Table 1). As mentioned earlier, we chose to solve the inner system less accurate when considering multiple time steps in parallel in the linear case. This results in more outer iterations needed for the first time step and consequently the right-hand-side is updated more frequently resulting in a better preconditioned next time step. This can especially be seen for  $s = 2$  where the number of outer iterations increases and at the same time the number of inner iterations decreases significantly which yields to an overall speedup of 1.8 which is nearly optimal.

In the nonlinear case one observes that the total number of inner and outer iterations were reduced with more parallelization, i.e. for the diffusion-reaction example both iteration counts were overall reduced by 60 – 70%. For  $s = 2$  the obtained reduction of 48% is nearly optimal (see Table 2). Larger  $s$  only yield a moderate benefit which can be explained by Figure 7a where it is shown that even for  $s = 2$  some time steps already converge after a single outer iteration and hence there cannot be much more benefit. Similar results can be seen for Richards’ equation (Table 4). Again outer and inner iteration counts were reduced by 60 – 70%. As before, for  $s = 2$  the reduction in inner and outer iterations is nearly optimal but for larger  $s$  the benefit is only moderate. Most likely this is caused by the larger splitting error and by the influence of the nonlinearity.

Figures 5, 7 and 10 show the evolution of inner and in the nonlinear case outer iterations per time step. After populating the pipeline, all experiments show a reduction in both iteration counts. The reason for this is that a time step, when newly shifted to the first column during the pipelining procedure, has an improved initial guess due to the previous approximate Newton updates before. However, this effect depends on the nonlinearity which can be seen e.g. for the Richards’ equation. Although, for larger  $s$  we still get a reduction in the iteration numbers, the benefit is only moderate.

Figure 7a shows that in the nonlinear diffusion-reaction example one actually reaches the behaviour mentioned in Remark 6, with sufficient parallelization the pipelining procedure only requires one Newton iteration per timestep.

Looking at the linear solver times in Tables 1, 2 and 4 one observes that for the nonlinear examples the best results are obtained for  $s = 4$ . For instance, the increased arithmetic intensity and vectorization yield a speedup of 2.6 for the Richards’ equation and for the preconditioner set up time a speedup of 2.9 is reached. In the linear case the best speedup is gained for  $s = 2$ . The optimal speedup is limited by the maximum of 8 vector lanes on *Intel Xeon Gold 6148* with *AVX512*. For values of  $s$  larger than 4 the measured times increase and in the nonlinear diffusion-reaction example for  $s = 16$  it is even more time needed than for  $s = 1$ , although the least iterations are needed. This is supposed to be caused by the worse cache behaviour mentioned in Section 3.

## 5 Conclusion

In this paper we presented a new generic framework for stiffly accurate diagonally implicit Runge-Kutta methods based on Parallel in Time ideas that makes use of the advantages of Block Krylov solvers. Furthermore, multiple properties of modern hardware like the use of SIMD-instructions and the efficient use of memory-bandwidth are respected. This is done by transforming a system for multiple consecutive time steps or Runge-Kutta stages into a single matrix equation that can be solved using a vectorized linear solver. By this the arithmetic intensity in the solver was increased. Hence, the framework is particularly well suited for low-order methods that are widely used in applications to porous media problems. The results show that the solver time of the linear solver was reduced by a factor of 2 – 3. The total number of linear solver iterations was reduced by around 60 – 70%. This means that the communication overhead on distributed systems would also be reduced by this factor. Due to its structure our approach is applicable for a wide class of linear and nonlinear problems.

Two aspects are important regarding the performance of the method and thus its applicability to other problems. The first aspect is the splitting error. Reducing it would reduce the number of outer iterations and by this improve the performance of the method. In particular in the nonlinear case this question is tightly related to the dynamics of the nonlinear operator. An analysis of the splitting error in this case would allow for a better a-priori estimate of the potential benefit of this type of parallelization.

A second aspect is the inherently sequential nature of problem, which becomes visible in the numerical experiments. With increasing parallelism, i.e. more time steps, the method becomes effectively slower again. In PinT methods a common approach is to use a discretization with coarser time steps and by this improve the overall convergence. Such ideas are employed in different ways in most parallel in time methods, c.f. [10], a future aim should thus be to also introduce such concepts into the presented method, in order to allow for more parallel stages.

## References

- [1] Hans Wilhelm Alt and Stephan Luckhaus. “Quasilinear elliptic-parabolic differential equations”. In: *Math. z* 183.3 (1983), pp. 311–341. DOI: 10.1007/BF01176474.
- [2] P. Bastian, F. Heimann, and S. Marnach. “Generic implementation of finite element methods in the Distributed and Unified Numerics Environment (DUNE)”. In: *Kybernetika* 46 (2010), pp. 294–315.
- [3] Peter Bastian, Mirco Altenbernd, Nils-Arne Dreier, Christian Engwer, Jorrit Fahlke, René Fritze, Markus Geveler, Dominik Göttsche, Oleg Iliev, Olaf Ippisch, et al. *Exa-Dune-Flexible PDE Solvers, Numerical Methods and Applications*. 2020. DOI: 10.1007/978-3-030-47956-5\_9.
- [4] Peter Bastian, Markus Blatt, Andreas Dedner, Nils-Arne Dreier, Christian Engwer, René Fritze, Carsten Gräser, Christoph Grüninger, Dominic Kempf, Robert Klöforn, et al. “The Dune framework: Basic concepts and recent developments”. In: *Computers & Mathematics with Applications* 81 (2021), pp. 75–112.
- [5] Peter Bastian, Markus Blatt, Andreas Dedner, Christian Engwer, Robert Klöforn, Ralf Kornhuber, Mario Ohlberger, and Oliver Sander. “A generic grid interface for parallel and adaptive scientific computing. Part II: implementation and tests in DUNE”. In: *Computing* 82 (2008), pp. 121–138.
- [6] K Dekker. “Partitioned Krylov subspace iteration in implicit Runge–Kutta methods”. In: *Linear algebra and its applications* 431.3-4 (2009), pp. 488–494. DOI: 10.1016/j.laa.2009.03.015.
- [7] Hans-Jörg G Diersch. *FEFLOW: finite element modeling of flow, mass and heat transport in porous and fractured media*. Berlin, Heidelberg: Springer, 2013. DOI: 10.1007/978-3-642-38739-5.
- [8] Nils-Arne Dreier and Christian Engwer. “Strategies for the vectorized block conjugate gradients method”. In: *Numerical Mathematics and Advanced Applications ENUMATH 2019: European Conference, Egmond aan Zee, The Netherlands, September 30-October 4*. Springer. 2020, pp. 381–388. DOI: 10.1007/978-3-030-55874-1\_37.
- [9] Christian Engwer, Patrick Henning, Axel Målqvist, and Daniel Peterseim. “Efficient implementation of the localized orthogonal decomposition method”. In: *Computer Methods in Applied Mechanics and Engineering* 350 (2019), pp. 123–153. DOI: 10.1016/j.cma.2019.02.040.
- [10] Martin J. Gander, Shu-Lin Wu, and Tao Zhou. *Time parallelization for hyperbolic and parabolic problems*. 2025. arXiv: 2503.13526 [math.NA]. URL: <https://arxiv.org/abs/2503.13526>.
- [11] Zachary J Grant. “Perturbed Runge–Kutta methods for mixed precision applications”. In: *Journal of Scientific Computing* 92.1 (2022), p. 6.
- [12] Laura Grigori, Sophie Moufawad, and Frédéric Nataf. “Enlarged Krylov subspace conjugate gradient methods for reducing communication”. In: *SIAM Journal on Matrix Analysis and Applications* 37.2 (2016), pp. 744–773. DOI: 10.1137/140989492.
- [13] Nicholas J Higham and Theo Mary. “Mixed precision algorithms in numerical linear algebra”. In: *Acta Numerica* 31 (2022), pp. 347–414. DOI: 10.1017/S0962492922000022.
- [14] Johannes Hofmann, Christie L Alappat, Georg Hager, Dietmar Fey, and Gerhard Wellein. “Bridging the architecture gap: Abstracting performance-relevant properties of modern server processors”. In: *Supercomputing Frontiers and Innovations* 7.2 (June 2020). ISSN: 2313-8734. DOI: 10.14529/jsfi200204.
- [15] Thomas Y Hou and Xiao-Hui Wu. “A multiscale finite element method for elliptic problems in composite materials and porous media”. In: *Journal of computational physics* 134.1 (1997), pp. 169–189. DOI: 10.1006/jcph.1997.5682.

- [16] Yoojin Jung, George Shu Heng Pau, Stefan Finsterle, and Ryan M Pollyea. “TOUGH3: A new efficient version of the TOUGH suite of multiphase flow and transport simulators”. In: *Computers & Geosciences* 108 (2017), pp. 2–7. DOI: 10.1016/j.cageo.2016.09.009.
- [17] Timo Koch, Dennis Gläser, Kilian Weishaupt, Sina Ackermann, Martin Beck, Beatrix Becker, Samuel Burbulla, Holger Class, Edward Coltman, Simon Emmert, et al. “DuMux 3—an open-source simulator for solving flow and transport problems in porous media with a focus on model coupling”. In: *Computers & Mathematics with Applications* 81 (2021), pp. 423–443. DOI: 10.1016/j.camwa.2020.02.012.
- [18] Olaf Kolditz, Sebastian Bauer, Lars Bilke, Norbert Böttcher, Jens-Olaf Delfs, Thomas Fischer, Uwe J Görke, Thomas Kalbacher, Georg Kosakowski, CI McDermott, et al. “OpenGeoSys: an open-source initiative for numerical simulation of thermo-hydro-mechanical/chemical (THM/C) processes in porous media”. In: *Environmental Earth Sciences* 67 (2012), pp. 589–599. DOI: 10.1007/s12665-012-1546-x.
- [19] Florian List and Florin A Radu. “A study on iterative methods for solving Richards’ equation”. In: *Computational Geosciences* 20 (2016), pp. 341–353. DOI: 10.1007/s10596-016-9566-3.
- [20] Kathryn Lund. “A new block Krylov subspace framework with applications to functions of matrices acting on multiple vectors”. PhD thesis. Temple University, 2018.
- [21] M Stuart Lynn, ACL Barnard, JH Holt, and LT Sheffield. “A proposed method for the inverse problem in electrocardiology”. In: *Biophysical journal* 7.6 (1967), pp. 925–945. DOI: 10.1016/S0006-3495(67)86630-x.
- [22] Per-Gunnar Martinsson and Joel A Tropp. “Randomized numerical linear algebra: Foundations and algorithms”. In: *Acta Numerica* 29 (2020), pp. 403–572. DOI: 10.1017/S0962492920000021.
- [23] Dianne P O’Leary. “The block conjugate gradient algorithm and related methods”. In: *Linear algebra and its applications* 29 (1980), pp. 293–322. DOI: 10.1016/0024-3795(80)90247-5.
- [24] Iuliu Sorin Pop, FLORIN Radu, and Peter Knabner. “Mixed finite elements for the Richards’ equation: linearization procedure”. In: *Journal of computational and applied mathematics* 168.1-2 (2004), pp. 365–373. DOI: 10.1016/j.cam.2003.04.008.
- [25] Florin A Radu, Iuliu Sorin Pop, and Peter Knabner. “Newton—type methods for the mixed finite element discretization of some degenerate parabolic equations”. In: *Numerical Mathematics and Advanced Applications: Proceedings of ENUMATH 2005, the 6th European Conference on Numerical Mathematics and Advanced Applications Santiago de Compostela, Spain, July 2005*. Springer, 2006, pp. 1192–1200. DOI: 10.1007/978-3-540-34288-5\_120.
- [26] Atgeirr Flø Rasmussen, Tor Harald Sandve, Kai Bao, Andreas Lauser, Joakim Hove, Bård Skaflestad, Robert Klöfkorn, Markus Blatt, Alf Birger Rustad, Ove Sævareid, et al. “The open porous media flow reservoir simulator”. In: *Computers & Mathematics with Applications* 81 (2021), pp. 159–185. DOI: 10.1016/j.camwa.2020.05.014.
- [27] Michael Rullmann, Alfred Anwander, Moritz Dannhauer, Simon K Warfield, Frank H Duffy, and Carsten H Wolters. “EEG source analysis of epileptiform activity using a 1 mm anisotropic hexahedra finite element head model”. In: *NeuroImage* 44.2 (2009), pp. 399–410. DOI: 10.1016/j.neuroimage.2008.09.009.
- [28] Eckhard Schneid. “Hybrid-gemischte Finite-Elemente-Diskretisierung der Richards-Gleichung”. PhD thesis. Naturwissenschaftliche Fakultät der Friedrich-Alexander-Universität Erlangen, 2000.
- [29] Marián Slodicka. “A robust and efficient linearization scheme for doubly nonlinear and degenerate parabolic problems arising in flow in porous media”. In: *SIAM journal on scientific computing* 23.5 (2002), pp. 1593–1614. DOI: 10.1137/S1064827500381860.
- [30] M Th Van Genuchten. “A closed-form equation for predicting the hydraulic conductivity of unsaturated soils”. In: *Soil science society of America journal* 44.5 (1980), pp. 892–898. DOI: 10.2136/sssaj1980.03615995004400050002x.
- [31] Wen-An Yong and Iuliu Sorin Pop. *A numerical approach to porous medium equations*. University of Heidelberg: IWR, 1996.

## Statements and declarations

**Funding** This research was supported by the Deutsche Forschungsgemeinschaft (DFG, German Research Foundation) under Germany's Excellence Strategy EXC 2044 – 390685587, Mathematics Münster: Dynamics-Geometry-Structure and DFG projects 504505951 (BlockXT - Block methods to transparently accelerate and vectorise time dependent simulations) and 230658507 (EXA-DUNE - Flexible PDE Solvers, Numerical Methods, and Applications).

**Competing interests** The authors have no relevant financial or non-financial interests to disclose.